RESEARCH ARTICLE

Editorial Process: Submission:01/27/2022 Acceptance:05/22/2022

Effects of Hypericin Encapsulated on Pluronic F127 Photodynamic Therapy Against Triple Negative Breast Cancer

Maria VF de Souza[1], Cristiane S Shinobu-Mesquita[1], Lyvia EF Meirelles[1], Natália L Mari[1], Gabriel B César[2], Renato S Gonçalves[2], Wilker Caetano[1], Edilson Damke[1], Vânia RS Silva[1], Gabrielle MZF Damke[1], Marcia EL Consolaro[1]*

Abstract

Objective: Breast cancer (BC) currently has no effective treatment especially for the highly aggressive and metastatic triple negative breast cancer (TNBC). Here, we investigated the antitumoral and antimigratory effects of hypericin (HYP) encapsulated on Pluronic F127 (F127/HYP) photodynamic therapy (PDT) against TNBC cell line MDA-MB-231 compared to a nontumorigenic human breast ductal cell line (MCF-10A). **Methods:** The phototoxicity/cytotoxicity was assessed by MTT assay, long-term cytotoxicity by clonogenic assay, cell uptake, subcellular distribution, and cellular oxidative stress by fluorescence microscopy, cell death with annexin V-FITC/propidium iodide, PDT mechanism using sodium azide and D-mannitol, and cell migration by wound-healing assay. **Results:** The treatment promoted phototoxic effect on tumor cell line in a dose-dependent and selective manner. Internalization of F127/HYP was efficient and accumulation occurred in the endoplasmic reticulum and mitochondria, resulting in cellular oxidative stress mainly by the type II mechanism, induced by necrosis. Furthermore, F127/HYP decreased colony formation and reduced the cell migration ability in MDA-MB-231 cells. **Conclusion:** Our results suggest a potentially useful role of F127/HYP micelles as a platform for HYP delivery to more specifically and effectively treat TNBC.

Keywords: Triple negative breast cancer- Hypericin- Micelles- Photodynamic therapy- Pluronic F127

Asian Pac J Cancer Prev, **23 (5)**, 1741-1751

Introduction

Breast cancer (BC), one of the leading causes of death among women is a complex disease in which genetic, epigenetic and environmental factors are implicated in its initiation and progression (Al-Alem et al., 2021). BC is also a heterogeneous disease that can be subdivided depending on the enrichment status of hormone receptors and human epidermal growth factor receptor 2 (HER2), respectively. Consequently, breast tumors can be categorized into four different groups: (1) hormone receptors positive with HER2 receptor-negative (Luminal A); (2) hormone receptors negative with HER2 receptor-positive (HER2 enriched); (3) positive for hormone receptors and HER2 receptor (Luminal B) and (4) triple-negative tumors (TNBC) which lack the expression of any of the receptors mentioned above (Elias, 2010). TNBC is infamously related to an increased rate of distant metastasis, recurrence, poor prognosis and a decreased overall and disease-free survival (Rakha et al., 2007). TNBC accounts for 15-20% of all BC cases (Anders and Carey, 2009) and currently, the only available treatments against TNBC are limited to chemotherapy, radiation and surgery (Willers et al., 1997; Kutanzi et al., 2011), being chemotherapy the most employed choice (Theodossiou et al., 2019). However, the lack of estrogen receptor (ER) has rendered TNBC insensitive to treatments with antiestrogens, such as the selective ER modulator tamoxifen, which is widely used in BC chemoprevention (Fisher et al., 1998; Radmacher and Simon, 2000), but also as an adjuvant to primary disease (Love, 1989; Thomas et al., 1992). Despite the existence of good other chemotherapeutic agents most fail to differentiate between healthy cells and malignant cells, resulting in systemic toxicity and severe side effects (Love, 1989). Therefore, it is critical to develop more effective and less toxic strategies for anti-BC therapies, especially TNBC.

Among the most promising modern cancer therapies alternatives, photodynamic therapy (PDT) is particularly attractive. PDT employs a photosensitizer (PS) that upon irradiation at a specific wavelength, generates single oxygen species and other free radicals, leading to cell death via autophagy, necrosis or apoptosis (Firczuk et al.,

*[1]Department of Clinical Analysis and Biomedicine, Clinical Cytology Laboratory, State University of Maringá (UEM), Paraná, Brazil. [2]Department of Chemistry, State University of Maringá, Av. Colombo, 5790, 87025-210, Maringá, Paraná, Brazil. *For Correspondence: melconsolaro@gmail.com*

2011). PDT is highly selective because photochemical reactions are extremely localized bringing significant clinical advantages compared to conventional cancer therapies (Dolmans et al., 2003; Firczuk et al., 2011).

Among prospective PS, Hypericin (HYP) is attractive because of a higher PDT response (Hudson et al., 1991; Falk and Schoppel, 1992; Chung et al., 1994; Falk, 1999). This property, together with minimal toxicity in the absence of light, selectivity for some tumors and a high clearance rate from the human organism, shows that HYP is a promising PS for PDT of cancer (Agostinis et al., 2002; Kiesslich et al., 2006; Karioti and Bilia, 2010). However, the use of HYP in PDT is limited because of the high hydrophobicity and aggregation in aqueous media and body fluid (Wirz et al., 2002; Kubin et al., 2008). It is thus essential to use drug delivery systems (DDSs) to overcome this shortcoming (Saw et al., 2006; Tatischeff et al., 2011).

Pluronic copolymers, like Pluronic F127 and P123 are well known in the biomedical field (Alexandridis et al., 1994). These copolymeric micelles are important to solubilize, protect and increase the bioavailability of the encapsulated compound (Kabanov et al., 2002; Sezgin et al., 2006; Swain et al., 2016). Pluronic F127 is considered one of the most suitable for biomedical applications due to its low toxicity and ability to encapsulate hydrophobic agents (Alakhov et al., 1996). Additionally, F127 enhances pro-apoptotic signaling, thereby sensitizing tumor cells and making them more vulnerable to the effects of anticancer drugs (Alakhov et al., 1996; Melik-Nubarov et al., 1999; Kabanov et al., 2002). Despite our previous studies presented the high efficiency of HYP-loaded pluronic P123 against Caco-2, MCF-7, HeLa, SiHa, CasKi and C33A cells (Montanha et al., 2017; Damke et al., 2020a; Damke et al., 2020b), as far as we know, the activity of HYP encapsulated with F127 (F127/HYP) against TNBC is unknown.

To continue and expand our studies, we investigated the effects of HYP encapsulated on Pluronic F127 (F127/HYP) PDT inBC cell line MDA-MB-231 (triple negative tumor cell/TNBC) compared to a nontumorigenic human breast ductal normal cell line (MCF-10A).

Materials and Methods

Photodrug synthesis andpreparation of HYP-loaded Pluronic F127 micelles

HYP was synthesized by Research Nucleus in Photodynamic Systems and Nanomedicine (NUPESF) in accordance with the previous report (Gonçalves et al., 2017). The nanoencapsulation of HYP in F127 copolymeric micelles was performed by the solid dispersion method (Zhang et al., 1996). Briefly, HYP and copolymer were initially solubilized in ethanol. The HYP stock solution was standardized using UV-Vis spectroscopy (UV–Vis Beckman Coulter DU® 800, USA) according to the Lambert-beer law and the volume added to the F127 solution calculated to obtain the HYP concentration of 100 µmol/L in the formulation and the mass of F127 was added to obtain a concentration equal to 250 µmol/L. Then, a solid dispersion consisting of F127/HYP was obtained after ethanol removal using rotary evaporation under reduced pressure. The solid matrix was maintained for 24 h in a sterilized desiccator under reduced pressure before adding water and stirring for 2 h. The concentration of HYP in the aqueous formulation was monitored using UV-vis spectroscopy to certify reproducibility in the preparations. The F127/HYP (100 µmol/L HYP/250 µmol/L F127) formulation was lyophilized and hydrated with sterile phosphate buffered saline (PBS) immediately prior to each experiment.

Spectroscopic characterization of F127/HYP-loaded copolymeric micelles

To better evaluate the HYP molecular organization and to evaluate the incorporation into the copolymeric micelle of F127, electron absorption spectra and fluorescence emission spectra (λexc = 525 nm, slits 5/5, optical path 1.00 cm) were monitored at 30°C. Briefly, the same F127/HYP molar ratio was reproduced which HYP 2.5 µmol/L due to the sensibility limit of the Uv-vis spectroscopy (UV–Vis Beckman Coulter DU 800, USA) and fluorescence emission. The spectra were collected at 37°C and compared to spectrum exhibits solubilized in ethanol.

Light source

The cell culture plates were illuminated throughout their area with a light-source device with 66 light-emitting diode (LED) units emitting white light at 6.3 J/cm2 (wavelength range from 450 to 750 nm). All tests were performed in the dark.

Cell lines and culture conditions

Cells were cultivated in 25 cm2 tissue culture flasks at 37◦C in a humidified atmosphere containing 5% CO_2/95% air. MDA-MB-231 cells, a human breast invasive adenocarcinoma cell line (negative for estrogen, progesterone and HER2 receptors, TNBC), was obtained from the Cell Bank of Rio de Janeiro/Brazil and were cultured in DMEM supplemented with 10% fetal bovine serum (FBS) and 1% antibiotic/antimycotic. MCF-10A cells, a human breast ductal normal cell line (non-tumorigenic control cells), was donated by Dr. Marcelo Gialluisi Bonini (University of Illinois at Chicago, USA) were cultured in DMEM supplemented with 10% FBS, 1 % antibiotic/antimycotic, 20 ng/mL human epidermal growth factor, and 0.5 µg/mL hydrocortisone. Sub culturing of the cells was performed using 0.25% trypsin. All reagents were purchased from Sigma-Aldrich (USA).

Cytotoxicity and phototoxicity

Cell cytotoxicity and phototoxicity were evaluated by (3-(4,5-dimethylthiazol-2-yl)-2,5-diphenyltetrazolium bromide) (MTT) (Damke et al., 2020a). A total of 2.5×10^5 cells/mL (MDA-MB-231 and MCF-10A cells) were seeded per well in a 96-well plate and incubated overnight. At the end of each incubation period, cells were treated with different concentrations of F127/HYP (0.4 - 2.2 µmol/L HYP and 1 - 5.5 µmol/L F127) and incubated for 30 min in the dark to evaluate cytotoxicity. To evaluate the

phototoxicity after this incubation, the cells were exposed to a light source for 15 min and then incubated in the dark for 30 min. Cells treated with DMEM (non-treated: NT) or F127 alone (5.5 µmol/L) were used as controls. After the treatment, the cells were washed with 100 µL of PBS and 50 µL of MTT solution (2 mg/mL) was added to each well and incubated in the dark at 37°C with 5% CO_2 for 4 h. At the end of incubation the resulting formazan was dissolved in 150 µL of DMSO and the absorbance was measured at 570 nm using a microplate reader (Loccus, Cotia, Brazil). The inhibitory concentrations (IC), IC_{30} (concentration that inhibited cell growth by 30% compared to NT), IC_{50} (inhibited cell growth by 50%) and IC_{90} (inhibited cell growth by 90%) values were obtained by nonlinear regression analysis of the data using GraphPad Prism 6.0 (GraphPad Software, San Diego, USA).

Clonogenic assay

MDA-MB-231 cells were seeded in 6-well plates (0.6×10^3 cells/well) and cultured for 24 h. After, the cells were treated with F127/HYP (IC_{30} and IC_{50} values) for 30 min in the dark, illuminated for 15 min and then in the dark for 30 min, and maintained in culture for 7 and 14 days. The medium was replaced three times every week. Cells were further stained with crystal violet (0.5% w/v) for colonies counting. The results were calculated (number of colonies formed by NT cells /number of cells seeded) X 100 (Franken et al., 2006).

Cellular uptake and subcellular distribution

To cellular uptake, MDA-MB-231 (2.5×10^4 cells/mL) were seeded in a 24-well tissue culture plate and incubated overnight. Then, the cells were treated with F127/HYP or HYP alone (1 µmol/L HYP/dimethyl sulfoxide-DMSO) for 30 min. Fluorescence images were analyzed and acquired on an EVOS FL microscope (Life Technologies, USA) with an RFV (red) filter.

To subcellular distribution, after the same incubation period and conditions, MDA-MB-231 cells (1.5×10^5 cells/mL) were incubated for 1 h with specific subcellular probes (Invitrogen, USA) including MitoTracker (mitochondria), ER-tracker (endoplasmic reticulum), NucBlue (nucleus) and for 30 min with F127/HYP. Fluorescence images were acquired using an EVOS FL microscope (Life Technologies, USA) with a blue (DAPI), green (GFP) and red (RFP) filters.

Cell death pathways

Apoptosis and necrosis assays were assessed by Annexin V-FITC/propidium Iodide (PI) based on a previously described protocol with some modifications (Damke et al., 2020a). Fluorescence images were acquired on an EVOS FL microscope (Life Technologies, USA) to distinguish the apoptotic (green fluorescence) and necrotic cells (red fluorescence). Fluorescence intensity was measured by ImageJ software (v1.48, public domain, National Institute of Health, USA).

Detection of total ROS levels

Intracellular ROS levels were detected based on an increase in the fluorescence caused by the conversion of a non-fluorescent dye H2DCFDA to highly fluorescent 2',7'-dichlorofluorescein (DCF), based on a previously described protocol with some modifications (Damke et al., 2020a). The fluorescence was measured at 488/530 nm of excitation/emission using an inverted fluorescence microscope (EVOS FL, Life Technologies, USA).

Evaluation of the PDT mechanism

Sodium azide (SA) and D-mannitol (DM), a separately specific 1O2 and hydroxyl radicals, were used to perform these experiments. Briefly, the test was divided into three groups including: 1 - IC_{30} value of F127/HYP; 2 - IC_{30} value of F127/HYP and 20 mmol/L SA solution; and 3 - IC_{30} value of F127/HYP and 40 mmol/L DM solution (Damke et al., 2020b). The cells (2.5×10^5 cells/mL) were seeded in 96-well plates and incubed for 24 h. Cell viability was determined by MTT assay.

Wound-healing migration assay

MDA-MB-231 cells (2.5×10^4 cells/mL) were seeded in 6-well tissue culture plates for 24 h. The cells were scratched with a sterile 1,000 µL pipette tip, washed with PBS and treated with IC_{30} and IC_{50} values of F127/HYP (30 min in the dark, illuminated for 15 min and then in the dark for 30 min). Cell migration was observed under an inverted microscope (EVOS FL, Life Technologies, USA; 5× magnification). Calculations were performed using the following formula: (Wound healing, WH % area) = [(Sample*100)]/Negative control at 0 h, 24 h, and 48 h (Liang et al., 2007).

Statistical analysis

Results were expressed as the mean ± SD from three independent experiments in triplicates. The data were analyzed using GraphPad Prism® 6 through one-way ANOVA for different groups followed by Tukey's–Kramer multiple range test. $P < 0.05$ was accepted as statistically significant.

Results

Spectroscopic characterization of HYP-loaded copolymeric micelles of F127

After HYP incorporation in the F127 copolymeric micelles, the resulting formulation with a concentration of 100 µmol/L HYP/250 µmol/L F127 was analyzed by fluorescence and spectroscopy to elucidate its monomeric form, in comparison to HYP in ethanol whenever necessary. The interactions with light enable data acquisitions at the molecular level about the HYP molecular organization. Intermolecular interactions and self-aggregation can be monitored through electronic absorption spectra and fluorescence emission of the HYP-loaded F127 copolymeric micelles. Figure 1 shows UV-Vis spectra of HYP solubilized in ethanol and nanoencapsulated in the F127 copolymeric micelles at 30°C.

The spectral profile similarity of HYP exhibited in ethanol and formulated with F127 indicates its predominance of soluble form in the nanostructured copolymeric micelles. Also, the spectroscopic characteristics of HYP formulated in copolymeric micelles

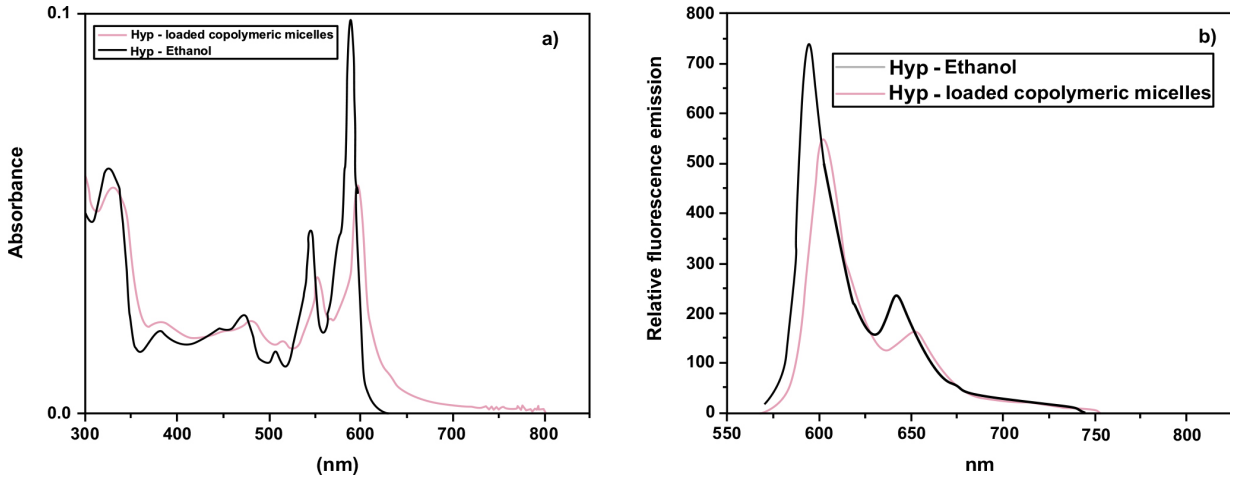

Figure 1. UV-Vis Spectra of HYP Solubilized in Ethanol and Nanoencapsulated in the Copolymeric Micelles of F127. (A) The UV–Vis electronic absorption and in (B) the fluorescence emission (λexc = 525 nm, slits 5/5, optical path 1.00 cm, pH 6.1 ± 0.3 at 30 °C). Spectral profile of absorbance and emission of HYP (100 µmol/L) solubilized in ethanol and formulated in the F127 copolymeric micelles (250 µmol/L).

of F127 indicated the solubilization of HYP.

Cell viability analysis of tumoral and non-tumoral cell lines after treatment

Since the HYP was efficient solubilized after incorporation in the F127 copolymeric micelles, it may be used as a potential anticancer agent. To study the effects of F127/HYP PDT against tumor cells as well as in normal cells, we exposed MDA-MB-231 cells (TNBC) compared to a non-tumorigenic human breast ductal cell line (MCF-

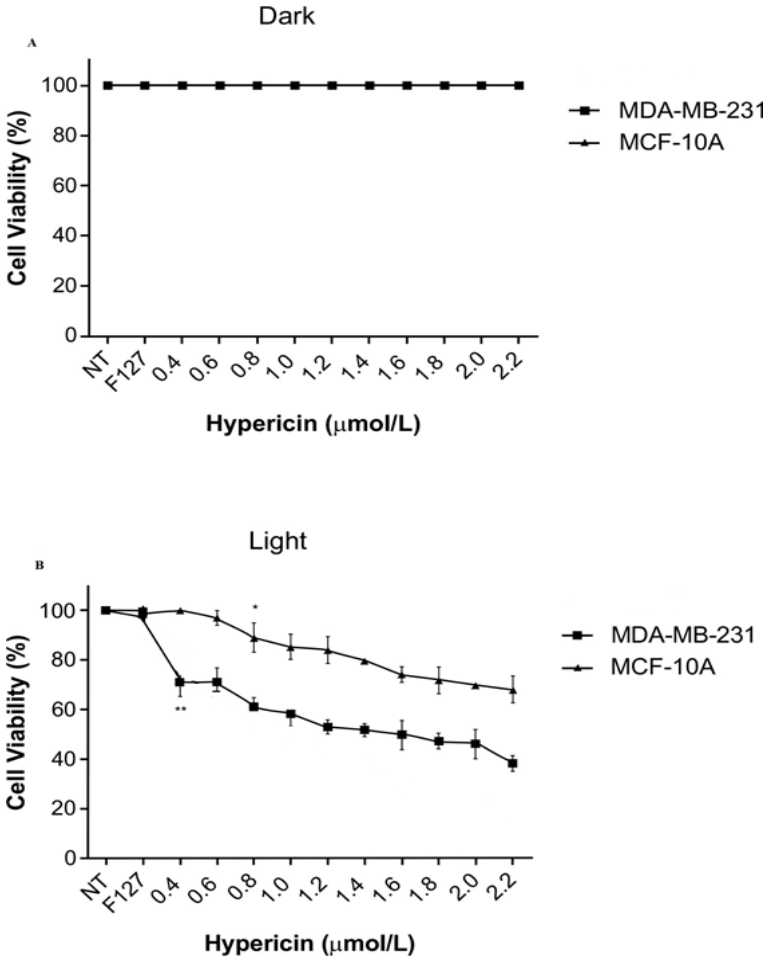

Figure 2. Cytotoxicity and Phototoxicity of F127/HYP Micelles (µmol/L) on MDA-MB-231 and MCF-10A Cell Lines, Evaluated by MTT Assay. (A) Graph of cytotoxicity indicating that the viability of MDA-MB-231 and MCF-10A cells after exposure to F127/HYP in the absence of light did not change. (B) Graph of phototoxicity showing a significant decrease in MDA-MB-231 cell viability, more than in MCF-10A cells. *, **, ***P < 0.05 vs NT was considered significant.

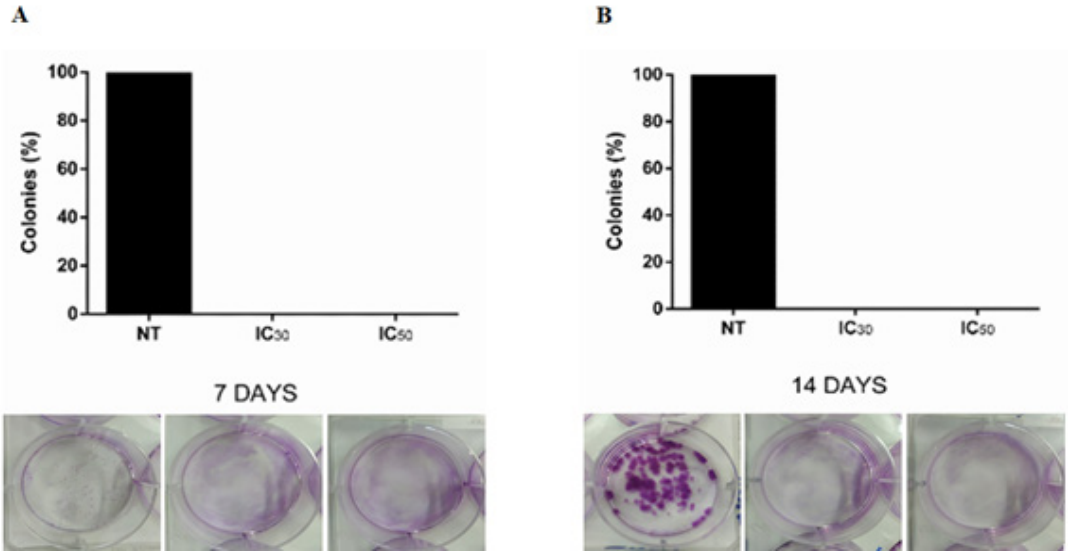

Figure 3. The Effect of Exposure to F127/HYP PDT in MDA-MB-231 Clonogenicity in 7 (A) and in 14 (B) Days. The photos indicate that the exposure to F127/HYP PDT completely inhibited the formation of MDA-MB-231 colonies. The (****) marks statistical significance when comparing groups of treated cells (IC_{30} and IC_{50}) with NT for 7 or 14 days. ****P <0.05 was considered significant.

10A), to increasing doses of F127/HYP in the absence of light (Figure 2A) or under light illumination (Figure 2B), which were evaluated by MTT assay. Overall, the solution containing only the F127 copolymer did not present any cytotoxic effect to the cells in the presence (Figure 2B) and absence of light (Figure 2A). The same occurred in all the cell lines exposed to the light without the presence of F127/HYP (NT), indicating that the illumination itself does not cause cytotoxic effects to the tested cells (Figure 2B). As seen in Figure 2A, when the cytotoxicity (absence of light) of F127/HYP was evaluated, there was no decrease in cell viability in all cell lines. On the other hand, F127/HYP micelles presented a significant dose-dependent cytotoxic effect against tumor cells after illumination but not on normal cells (Figure 2B). More specifically, the phototoxic effect was observed from the first concentration tested (0.4 µmol/L) in MCF-7 (P =0.0003) and MDA-MB-231 (P =0.0010) tumor cells. In addition, in the non-tumor cell line MCF-10A, the viability decreased significantly only from the third concentration tested (0.8 µmol/L, P =0.0270) but was not sufficient for the calculation of IC values, which were > 2.2 µmol/L. Taken together, these data indicate that F127/HYP PDT exerted selective concentration-dependent phototoxic effects against the tumor cell line tested, with an IC_{50} of 2.0 µmol/L for MDA-MB-231 cells (Table 1).

Next, the clonogenic cell survival assay was performed to analyze the ability of the cells to proliferate indefinitely, thereby retaining the reproductive ability to form a large colony or a clone after F127/HYP PDT. For MDA-MB-231 cell line, the clonogenic potential was significantly reduced at the tested concentrations (P <0.0001) after illumination for 7 and 14 days of incubation with IC_{30} and IC_{50} compared to NT. Additionally, the reduction was complete, with no colony growth after treatment (Figure 3).

F127/HYP cells internalization and subcellular localization after treatment

In The presence of intracellular F127/HYP was observed through the emitted fluorescence in the RFV (red) filter, as seen in Figure 4. It was possible to observe

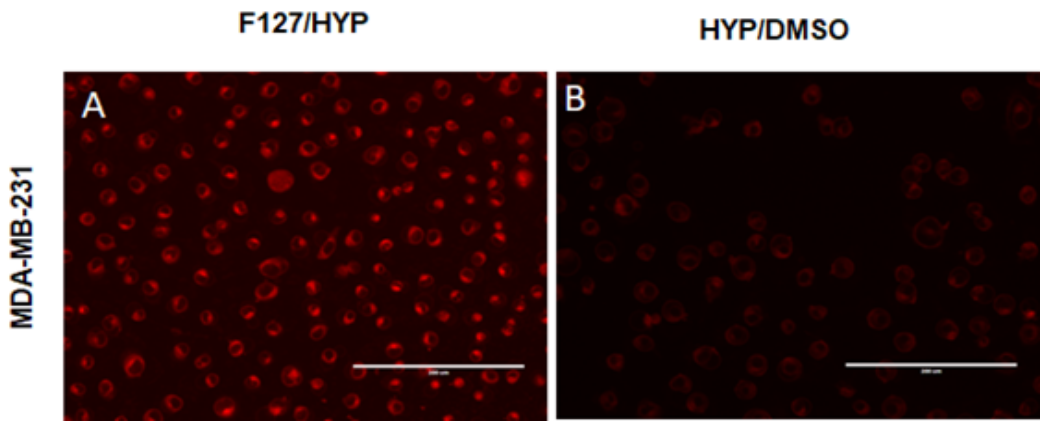

Figure 4. Intracellular Uptake of F127/HYP was Visualized by Fluorescence Inverted Microscopic with RFV (red) Filter after Incubating MDA-MB-231 Cells with F127/HYP (A) or HYP/DMSO (B) for 30 min (20x magnification).

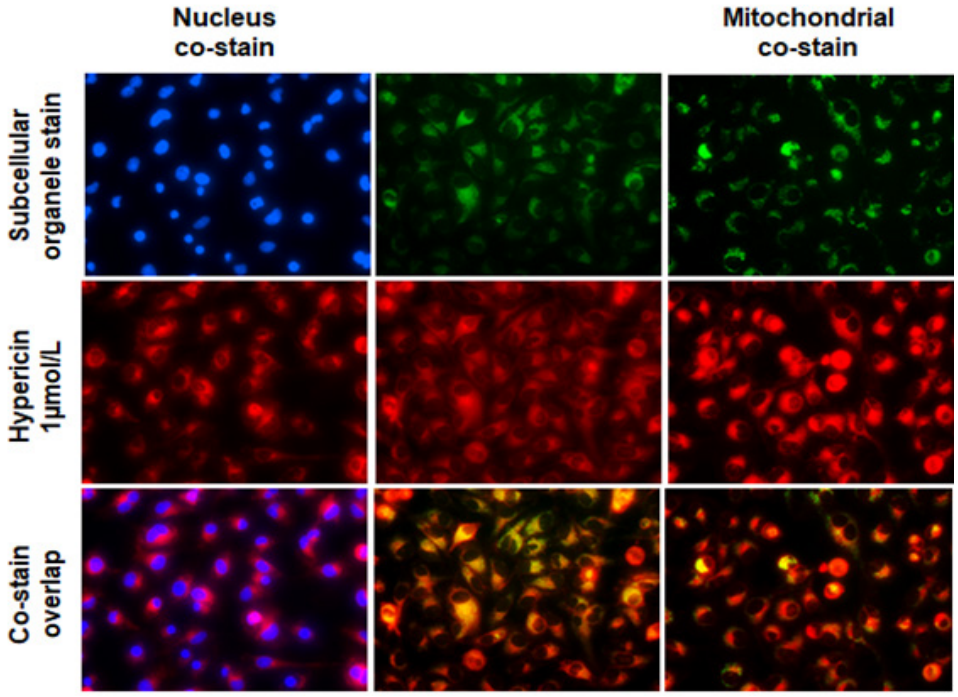

Figure 5. HYP Subcellular Localization in MDA-MB-231 Cells after Treatment with F127/HYP Micelles for 30 min and co-Stained with Specific Organelle Probes for Mitochondria (MitoTracker, green), Endoplasmic Reticulum (ER-tracker, green), and Nucleus (NucBlue, blue). Fluorescence imaging and photomicrographs at 20x magnification.

that the intensity of the emitted fluorescence by HYP on tumor cell line treated with F127/HYP micelles (Figure 4A) was higher than treated with free HYP (solubilized in DMSO) (Figure 4B). In addition, fluorescence was observed in the cytoplasm of tumor cells (Figure 4A). When the cells were exposed to free HYP, it was not possible to verify red fluorescence inside the cells (Figures 4A-B).

The subcellular localization of F127/HYP in MDA-MB-231 cells was analyzed by specific probes for

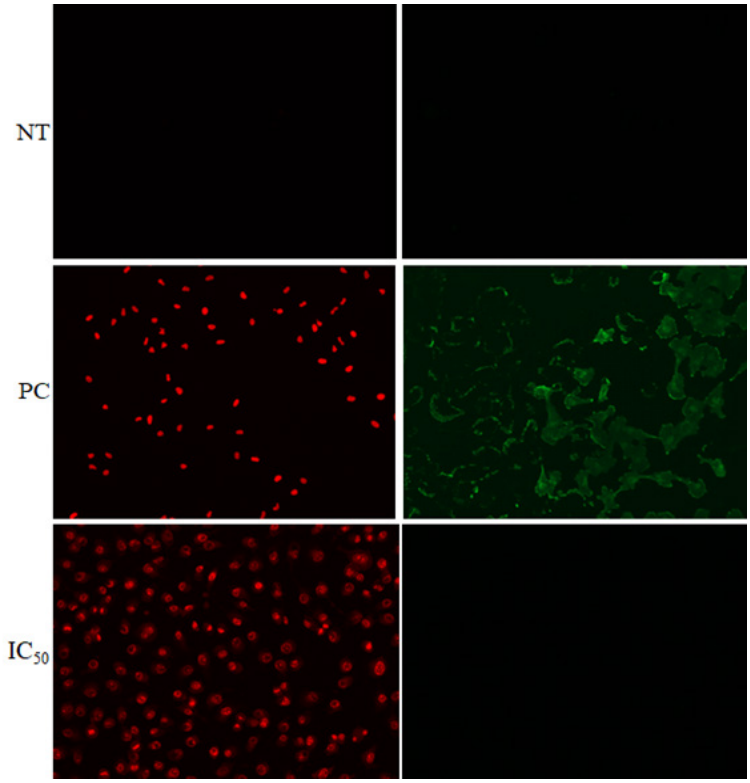

Figure 6. Death Pathways Induced by F127/HYP PDT in MDA-MB-231 Cells. Representative figures of MDA-MB-231 cells exposed to F127/HYP (IC50) after illumination that were stained with the apoptosis marker annexin V (green fluorescence) and the necrosis marker propidium iodide (PI) (red fluorescence). Positive (Camptothecin) and negative (Digitonin) controls were used for apoptosis and necrosis, respectively (20x magnification).

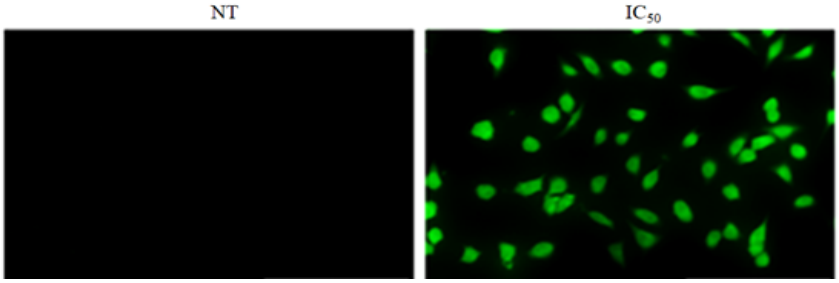

Figure 7. Total ROS Production Induced by F127/HYP PDT (IC_{50}) in the MDA-MB-231 Cells. The untreated (NT) tumor cells presented no fluorescence and there was no ROS production. The treated tumor cells presented high fluorescence, indicating the generation of ROS induced by F127/HYP PDT.

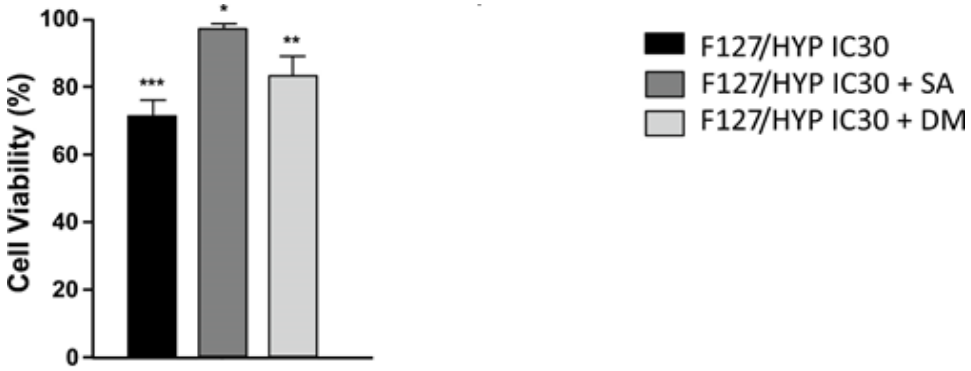

Figure 8. Cell Viability of F127/HYP IC30 Values of the Two Groups Tested with SA and DM was Higher than those Treated Only with F127/HYP IC30 Values. The (*) (**) (***) marks statistical significance and $P < 0.05$ was considered significant.

ER, mitochondria and nucleus. Figures 5 shows that the tumor cells presented high fluorescence of mitochondria and ER.

Table 1. Values of Inhibitory Concentrations (IC) According to Cell Viability Determined by MTT Assay.

Cell line	IC_{30} (µmol/L)	IC_{50} (µmol/L)	IC_{90} (µmol/L)
MDA-MB-231	1.20	2.00	3.60

Cell death induced by F127/HYP-mediated PDT

The occurrence of necrosis and/or apoptosis following PDT depends on HYP subcellular location (Thomas et al., 1992). Therefore, considering that HYP was sub-localized in the ER and mitochondria, we evaluated the

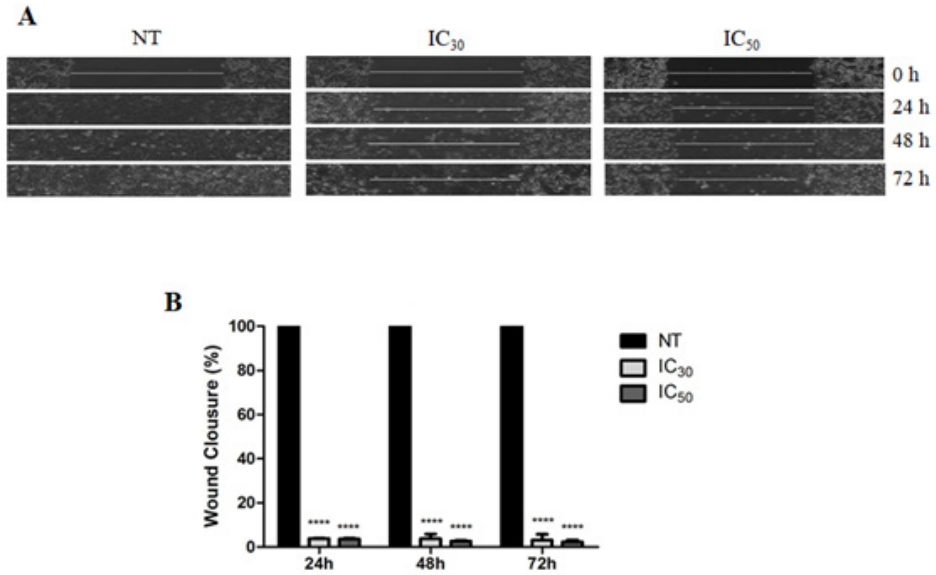

Figure 9. Effects of F127/HYP Exposure against Breast Cancer Cells Migration. (A) MDA-MB-231 cells after scratching in the absence (NT) and presence of F127/HYP (IC_{30} and IC_{50}) (20x magnification). (B) Graph shows the mean (%) of the results calculated by comparing the wound closure after 24, 48, and 72 h with the wound measurement at the initial time. *$P < 0.05$ was considered significant.

type and extent of cell death involved in cells treated with F127/HYP PDT via an Annexin V-FITC/PI fluorescence assay. PI detects necrosis (red fluorescence) and annexin-V detects apoptosis (green fluorescence). As shown in Figure 6, F127/HYP PDT exposition induced cell death by necrosis in MDA-MB-231 cells.

ROS production and PDT mechanism induced by F127/HYP

We first evaluated the total ROS production based on fluorescence emission, which is occasioned by the conversion of a non-fluorescent dye H_2DCFDA into DCF, which is fluorescent. Figure 7 shows the bright field images and their corresponding fluorescence images of the NT tumor cells that presented no fluorescence, indicating the absence of ROS production, thus, no oxidative stress. On the contrary, cells treated with 0.4 μmol/L of F127/HYP presented high fluorescence, indicating the high production of ROS.

In order to visualize the photochemical processes mechanism of F127/HYP PDT, SA and DM, a separately 1O2 scavengers and hydroxyl radicals (HR) scavengers were used to quench corresponding ROS of Type II and Type I originated from PDT and distinguish the two types of photodynamic reaction. When adding SA and DM into the culture medium, corresponding ROS generated from F127/HYP induced PDT process would be quenched, resulting in lower photodynamic activity and subsequently increasing cell viability (Liang et al., 2007). As shown in Figure 8, the cell viability of the two groups tested with SA or DM was higher than those treated only with F127/HYP IC_{30} values, suggesting that the key ROS have generated in both tumor cell lines after treatment with F127/HYP-PDT and been quenched effectively. In addition, the cell viability of F127/HYP -PDT-SA group was slightly higher than that of F127/HYP -PDT-DM group also in both tumor cell lines, suggesting that the production of singlet oxygen is more than that of oxygen-centered radicals.

Effects on cell migration after F127/HYP-mediated PDT

We evaluated the ability of BC cells treated with F127/HYP PDT to migrate using the wound-healing assay. The reduction in cell migration after treatment was significant at 24, 48 and 72 h at both concentrations tested (IC_{30} and IC_{50}) ($P < 0.0001$). The untreated MDA-MB-231 cells closed within 24 h (Figure 9).

Discussion

In this study, we investigated the effects of HYP encapsulated on Pluronic F127 (F127/HYP) PDT in BC cell line MDA-MB-231 (triple negative tumor cell/TNBC) compared to a nontumorigenic human breast ductal normal cell line (MCF-10A).

In relation to F127/HYP micelles, the spectroscopic characteristics of HYP formulated in copolymeric micelles of F127 indicated the solubilization of HYP and the promising application of this biocompatible copolymer as DDS for HYP.

In relation to i*n vitro* analyses, our results showed that F127/HYP micelles presented effective and selective time- and dose-dependent phototoxic effects against BC cells but little damage to normal cells (MCF-10A). These data highlight the selective effect of HYP micelles against cancer cells, similar to other *in vitro* (Chen and De Witte, 2000, Roelants et al., 2011, Vandepitte et al., 2011, Xu et al., 2019) and *in vivo* (Jedzelovská et al., 2016) studies. Additionally, our data are in agreement with our previous study in which HYP in P123 micelles PDT presented a selective effect in MCF-7 but not in MCF-10A normal cells (Damke et al., 2020a). Based on the investigation mentioned above, it is clear that F127/HYP presents a strong photodynamic activity with no dark toxicity and provides potential application in PDT against BC. Additionally, the results indicated that F127/HYP PDT decrease long-term cells proliferation, suggesting a possible ability to prevent the recurrence of TNBC. Taken together, these results show that F127/HYP micelles PDT presented a selective dose-time-dependent phototoxic effect and decreased colony formation on both tumor cells, highlighting their potential for PDT of TNBC.

In order to perform the in vivo PDT, the PS should be able to enter tumor cells. Cancer cells should uptake a PS successfully in PDT (Saw et al., 2006). Therefore it is vital to study the interaction between a F127/HYP and the cell membrane. Hydrophobicity of drugs has a great influence on cellular uptake and determines the ability of the drug to penetrate the cell membrane. In general, highly lipid soluble drugs can penetrate the cell membrane easily (Zeng et al., 2019). Our designed F127/HYP micelles presented selective internalization in the tumor cells. Based on this investigation, we inferred that F127/HYP micelles exhibited a higher capacity to permeate the cytoplasmic membrane and to internalize preferably in the cytoplasm of the tumor cells compared to free HYP. Thus, the entry of HYP into the TNBC was facilitated by the F127 (Saw et al., 2006).

Moreover, F127/HYP micelles accumulated in ER and mitochondria, resulting in cell death by necrosis. Crucial parameters to determine the photocytotoxic activity of HYP are the cell permeability and subcellular localization. It is clear that the final destination of HYP in the cell will determine its apical molecular targets and will influence the photocytotoxic profile. This is because, within the cellular milieu, $^1O_2$ and the majority of other ROS have extremely short lives and small radii of diffusion due to their rapid interaction with biological targets; this interaction ultimately leads to modification of the cellular functionality and potentially cell death (Theodossiou et al., 2009). Our data shows that the tumor cells presented high fluorescence of mitochondria and ER, in agreement with other studies (Agostinis et al., 2002, Kascakova et al., 2008, Theodossiou et al., 2009). Additionally, tumor cells not presented HYP fluorescence of the nucleus, as previously described (Agostinis et al., 2002).

Considering the results of cellular uptake and subcellular distribution of F127/HYP micelles, we can infer that the problem of HYP hydrophobicity (Wirz et al., 2002, Kubin et al., 2008) was efficiently overcomed with the Pluronic F127 encapsulation.

In relation to cells death, F127/HYP PDT exposition induced cell death by necrosis in MDA-MB-231 cells. It's already well-established that generally PSs located in the mitochondria or the ER promote apoptosis, within a certain threshold of oxidative stress, while PDT with PSs targeting either the plasma membrane or lysosomes can either delay or block the apoptotic program predisposing the cells to necrosis (Diwu and Lown, 1993). However, our result can be explained by the fact that depending on the strength of the photodynamic process (e.g., light dose and dye concentration) HYP may inflict severe damage to the mitochondria leading to a bioenergetic collapse which favors necrotic cell death or diminish their defenses against cell death pathways, perturbing the mitochondrial membrane integrity (Theodossiou et al., 2009). Furthermore, necrosis was the predominant death pathway due HYP PDT in our previous studies with HYP (Damke et al., 2020a, Damke et al., 2020b) and also in studies conducted by other authors (Okpanyi et al., 1990, Mikes et al., 2009).

Excessive ROS production during PDT leads to oxidative stress and may trigger the induction of apoptosis, necrosis or autophagy associated cell death. Our results indicating indicating the high production of ROS similar to the study of Damke et al., 2020a, with HYP/P123 PDT in MCF-7 cells.

Total ROS production due to PDT can occur through two mechanisms known as type I and type II. In type I pathway, the excited triplet state can react with the biomolecules by transferring charges, resulting in radicals and radical ions that react with molecular oxygen, leading to the generation of ROS including superoxide anions (O_2^-), singlet oxygen ($^1O_2$), hydroxyl radicals (HO) and hydrogen peroxide (H_2O_2). In type II pathway, the direct energy transfer occurs from the PS in the triplet excited state to the oxygen in the fundamental triplet state, producing $^1O_2$, a highly cytotoxic agent (Liang et al., 2007). In this sense, type II reaction played a predominant role in the process of F127/HYP induced PDT. Moreover, Type I and Type II photodynamic reactions can occur simultaneously in PDT process (Siboni et al., 2002, Mikes et al., 2007). However, direct and indirect evidence supports a prevalent role for $^1O_2$ in the molecular processes initiated by PDT (Niedre et al., 2002) as detected by us. Additionally, it has been suggested that the type II mechanism is the one to play a major role in the biological photoactivity of HYP, which is also in line with our results. Taken together, our data reinforced that the PDT activity using the F127/HYP increased cellular oxidative stress in the TNBC cell line mainly via type II mechanism of PDT.

Finally, F127/HYP micelles inhibited the migration and invasion of tumor cells, evidencing the potential of PDT with F127/HYP in preventing the migration of TNBC cells, possibly by decreasing their metastatic potential. This is an important finding because MDA-MB-231 cells are derived from TNBC, which is a highly aggressive and highly metastatic cancer (Anders and Carey, 2009) and F127/HYP PDT emerges as a very promising alternative for the treatment of this BC type.

In conclusion, this paper reports the in vitro PDT of HYP encapsulated on Pluronic F127 (F127/HYP) against MDA-MB-231 cells, compared to the nontumorigenic MCF-10A cells. Taken together, the results presented here indicate a potentially useful role of F127/HYP micelles as a valuable platform for HYP delivery to more specifically and effectively treat TNBC, by PDT.

Author Contribution Statement

MVF Souza, W Caetano, MEL Consolaro, GMZF Damke and F VRS da Silva designed and wrote the study protocol; MVF Souza, NL Mar, GB César, RS Gonçalves, LEF Meirelles, and GMZF Damke were in charge of analysis; MVF Souza, VRS da Silva, and CS Shinobu-Mesquita managed the data and performed the statistical analysis; and; MVF Souza, CS Shinobu-Mesquita, E Damke, VRS da Silva, W Caetano and MEL Consolaro wrote the manuscript. All of the authors have read and approved the final manuscript.

Acknowledgments

None.

Funding Statement

This study was supported by the Conselho Nacional de Desenvolvimento Científico e Tecnológico (CNPq) (grants 304037/2019-2 and 409382/2018-3) and Coordenação de Aperfeiçoamento de Pessoal de Nível Superior (Capes), for the scholarships.

This study was part of an approved student thesis (Maria Vitória de F. Souza).

Availability of data

All data generated or analyzed during this study are included in this published article.

Statement conflict of Interest

The authors declare no conflicts of interest or industry supports of the project in this study.

References

Agostinis P, Vantieghem A, Merlevede W, De Witte PA (2002). Hypericin in cancer treatment: more light on the way. *Int J Biochem Cell Biol*, **34**, 221-41.

Alakhov VY, Moskaleva EY, Batrakova EV, Kabanov AV (1996). Hypersensitization of multidrug resistant human ovarian carcinoma cells by pluronic P85 block copolymer. *Bioconjug Chem*, **7**, 209-16.

Al-Alem U, Mahmoud AM, Batai K, et al (2021). Genetic variation and immunohistochemical localization of the glucocorticoid receptor in breast cancer cases from the breast cancer care in Chicago cohort. *Cancers*, 3, 2261.

Alexandridis P, Holzwarth JF, Hatton TA (1994). Micellization of poly (ethylene oxide)-poly (propylene oxide)-poly (ethylene oxide) triblock copolymers in aqueous solutions: thermodynamics of copolymer association. *Macromol*, **27**, 2414-25.

Anders CK, Carey LA (2009). Biology, metastatic patterns, and

treatment of patients with triple-negative breast cancer. *Clin Breast Cancer*, **9**, S73-81.
Chen B,De Witte PA (2000). Photodynamic therapy efficacy and tissue distribution of hypericin in a mouse P388 lymphoma tumor model. *Cancer Lett*, **150**, 111-7.
Chung PS, Rhee CK, Saxton RE, et al (1994). Hypericin uptake in rabbits and nude mice transplanted with human squamous cell carcinomas: study of a new sensitizer for laser phototherapy. *Laryngoscope*, **104**, 1471-6.
Damke GMZF, Damke E, Bonfim-Mendonça PS, et al (2020). Selective photodynamic effects on cervical cancer cells provided by P123 Pluronic®-based nanoparticles modulating hypericin delivery. *Life Sci*, **255**, 117858.
Damke GMZF, Souza RP, Montanha MC, et al (2020). Selective photodynamic effects on breast cancer cells provided by P123 Pluronic®- based nanoparticles modulating hypericin delivery. *Anticancer Agents Med Chem*, **20**, 1352-67.
Diwu Z, Lown JW (1993). Photosensitization with anticancer agents 17. EPR studies of photodynamic action of hypericin: formation of semiquinone radical and activated oxygen species on illumination. *Free Radic Biol Med*, **14**, 209-15.
Dolmans DE, Fukumura D, Jain RK (2003). Photodynamic therapy for cancer. *Nat Rev Cancer*, **3**, 380-7.
Elias AD (2010). Triple-negative breast cancer: a short review. Am J Clin Oncol,33, 637–45. Haffty BG, Qyang Q, Reiss M, et al (2006). Locoregional relapse and distant metastasis in conservatively managed triple negative early-stage breast cancer. *J Clin Oncol*, **24**, 5652–7.
Falk H (1999). From the photosensitizer hypericin to the photoreceptor stentorin—the chemistry of phenanthroperylene quinones. *Angew Chem Int Ed Engl*, **38**, 3116-36.
Falk H, Schoppel G (1992). On the synthesis of hypericin by oxidative trimethylemodin anthrone and emodin anthrone dimerization: isohypericin. *Monatsh Chem*, **123**, 931-8.
Firczuk M, Nowis D, Gołąb J (2011). PDT-induced inflammatory and host responses. *Photochem Photobiol Sci*, **10**, 653-63.
Fisher B, Costantino JP, Wickerham DL, et al (1998). Tamoxifen for prevention of breast cancer: report of the National Surgical Adjuvant Breast and Bowel Project P-1 Study. *J Natl Cancer Inst*, **90**, 1371-88.
Franken NA, Rodermond HM, Stap J, et al (2006). Clonogenic assay of cells in vitro. *Nat Protoc*, **1**, 2315-09.
Gonçalves RS, Rabello RR, G.B. César GB, et al (2017). An efficient multigram synthesis of hypericin improved by a low power LED based photoreactor. *Org Process Res Dev*, **21**, 2025-31.
Hudson JB, Lopez-Bazzocchi I, Towers GHN (1991). Antiviral activities of hypericin. *Antiviral Res*, **15**, 101-12.
Jendželovská Z, Jendželovský R, Kuchárová B, Fedoročko P (2016). Hypericin in the light and in the dark: two sides of the same coin. *Front Plant Sci*, **7**, 560.
Kabanov AV, Batrakova EV, Alakhov VY (2002). Pluronic® block copolymers as novel polymer therapeutics for drug and gene delivery. *J Control Release*, **82**, 189-12.
Karioti A, Bilia AR (2010). Hypericins as potential leads for new therapeutics. *Int J Mol Sci*, **11**, 562-94.
Kascakova S, Nadova Z, Mateasik A, et al (2008). High level of low-density lipoprotein receptors enhance hypericin uptake by U-87 MG cells in the presence of LDL. *Photochem Photobiol*, **84**, 120-7.
Kiesslich T, Krammer B, Plaetzer K (2006). Cellular mechanisms and prospective applications of hypericin in photodynamic therapy. *Curr Med Chem*, **13**, 2189-04.
Kubin A, Loew HG, Burner U, et al (2008). How to make hypericin water-soluble. *Pharmazie*, **63**, 263-9.
Kutanzi KR, Yurchenko OV, Beland FA (2011). MicroRNA-mediated drug resistance in breast cancer. *Clin Epig*, **2**, 171-85.
Liang CC, Park AY, Guan JL (2007). In vitro scratch assay: a convenient and inexpensive method for analysis of cell migration in vitro. *Nat Protoc*, **2**, 329-33.
Love RR (1989). Tamoxifen therapy in primary breast cancer: biology, efficacy, and side effects. *J Clin Oncol*, **7**, 803-15.
Melik-Nubarov NS, Pomaz OO, Dorodnych TY, et al (1999). Interaction of tumor and normal blood cells with ethylene oxide and propylene oxide block copolymers. *FEBS Lett*, **446**, 194-8.
Mikeš J, Jendželovský R, Sačková V, et al (2009). The role of p53 in the efficiency of photodynamic therapy with hypericin and subsequent long-term survival of colon cancer cells. *Photochem Photobiol Sci*, **8**, 1558-67.
Mikeš J, Kleban J, Sačková V, et al (2007). Necrosis predominates in the cell death of human colon adenocarcinoma HT-29 cells treated under variable conditions of photodynamic therapy with hypericin. *Photochem Photobiol Sci*, **6**, 758-66.
Montanha MC, Silva LL, Pangoni FBB, et al (2017). Response surface method optimization of a novel hypericin formulation in P123 micelles for colorectal cancer and antimicrobial photodynamic therapy. *J Photochem Photobiol B*, **170**, 247-55.
Niedre M, Patterson MS, Wilson BC (2002). Direct near-infrared luminescence detection of singlet oxygen generated by photodynamic therapy in cells in vitro and tissues in vivo. *Photochem Photobiol*, **75**, 382-91.
Okpanyi SN, Lidzba H, Scholl HBC, Miltenburger HG (1990). Genotoxicity of a standardized hypericum extract. *Arzneimittelforschung*, **40**, 851-5.
Radmacher MD, Simon R (2000). Estimation of tamoxifen's efficacy for preventing the formation and growth of breast tumors. *J Natl Cancer Inst*, **92**, 48-53.
Rakha EA, El-Sayed ME, Green AR, et al (2007). Prognostic markers in triple-negative breast cancer. *Cancer*, **109**, 25–32.
Roelants M, Van Cleynenbreugel B, Lerut E, Van Poppel H, De Witte PA (2011). Human serum albumin as key mediator of the differential accumulation of hypericin in normal urothelial cell spheroids versus urothelial cell carcinoma spheroids. *Photochem Photobiol Sci*, **10**, 151-9.
Saw CLL, Olivo M, Soo KC, Heng PWS (2006). Delivery of hypericin for photodynamic applications. *Cancer Lett*, **241**, 23-30.
Sezgin Z, Yüksel N, Baykara T (2006). Preparation and characterization of polymeric micelles for solubilization of poorly soluble anticancer drugs. *Eur J Pharm Biopharm*, **64**, 261-8.
Siboni G, Weitman H, Freeman D, et al (2002). The correlation between hydrophilicity of hypericins and helianthrone: internalization mechanisms, subcellular distribution and photodynamic action in colon carcinoma cells. *Photochem Photobiol Sci*, **1**, 483-91.
Swain S, Sahu PK, Beg S, Babu SM (2016). Nanoparticles for cancer targeting: current and future directions. *Curr Drug Deliv*, **13**, 1290-02.
Tatischeff I, Alfsen A (2011). A new biological strategy for drug delivery: eucaryotic cell-derived nanovesicles. *J Biomater Nanobiotechnol*, **2**, 494.
Theodossiou TA, Ali M, Grigalavicius M, et al (2019). Simultaneous defeat of MCF7 and MDA-MB-231 resistances by a hypericin PDT–tamoxifen hybrid therapy. *NPJ Breast Cancer*, **5**, 1-10.
Theodossiou TA, Hothersall JS, De Witte PA, et al (2009). The multifaceted photocytotoxic profile of hypericin. *Mol Pharm*, **6**, 1775-89.
Thomas C, Macgill RS, Miller GC, Pardini RS (1992).

Photoactivation of hypericin generates singlet oxygen in mitochondria and inhibits succinoxidase. *Photochem Photobiol*, **55**, 47-53.

Vandepitte J, Roelants M, Van Cleynenbreugel B, et al (2011). Biodistribution and photodynamic effects of polyvinylpyrrolidone-hypericin using multicellular spheroids composed of normal human urothelial and T24 transitional cell carcinoma cells. *J Biomed Opt*, **16**, 018001.

Willers H, Würschmidt F, Janik I, et al (1997). Combined breast-preserving surgery, chemotherapy and radiotherapy in the treatment of breast carcinoma. Effect of the interval between surgery and the beginning of radiotherapy. *Strahlenther Onkol*, **3**, 148-54.

Wirz A, Meier B, Sticher O (2002). Solubility of hypericin in methanol and methanol-pyridine. *Pharmazie*, **57**, 543-5.

Xu L, Zhang X, Cheng W, et al (2019). Hypericin-photodynamic therapy inhibits the growth of adult T-cell leukemia cells through induction of apoptosis and suppression of viral transcription. *Retrovirol*, **16**, 1-13.

Zhang X, Jackson JK, Burt HM (1996). Development of amphiphilic diblock copolymers as micellar carriers of taxol. *Int J Pharm*, **132**, 195-06.

Zhanga R, Qina X, Fandong Kong F, et al (2019). Improving cellular uptake of therapeutic entities through interaction with components of cell membrane. *Drug Del*, **26**, 328–42.